

Cosmic dawn constraints on freeze-in dark matter from Lyman- α forest and 21-cm signal : single-field models

Zixuan Xu, Quan Zhou and Sibo Zheng

Department of Physics, Chongqing University, Chongqing 401331, China

Abstract

We propose cosmological observations of Lyman- α and 21-cm signal to set stringent constraints on freeze-in dark matter (FIDM). Explicitly we consider Higgs (neutrino)-portal FIDM in the single-field context, which injects energy into the intergalactic medium via its annihilation (decay). With respect to Lyman- α the baseline ionization history is inferred from low redshift data about astrophysical reionization, whereas for 21-cm signal the baseline values of 21-cm power spectrum are obtained through a standard modeling of star formation developed. We use numerical tools to derive the FIDM induced deviations from these baseline values in high redshift region. Our results show that (i) current Lyman- α data has already constrained the neutrino-portal FIDM mass to be less than 1.06 MeV, (ii) future Lyman- α data about the intergalactic medium temperature with a 10 (100)% precision at $z \sim 9 - 15$ is sufficient to exclude the Higgs (neutrino)-portal FIDM, and (iii) future SKA sensitivity (1000 hrs) on the 21-cm power spectrum for reference wavenumber $k_* = 0.2h \text{ Mpc}^{-1}$ at $z \sim 15 - 16$ is also able to exclude the surviving neutrino-portal FIDM mass window.

Contents

1	Introduction	1
2	Freeze-in dark matter induced energy injection into the IGM	3
2.1	Higgs portal	3
2.2	Neutrino portal	4
3	Modeling dark matter induced effects on cosmological observations	5
3.1	Lyman- α	5
3.2	21-cm signal	6
4	Results	8
4.1	Higgs portal	8
4.1.1	Lyman- α	8
4.2	Neutrino portal	10
4.2.1	Lyman- α	10
4.2.2	21-cm signal	12
5	Conclusion	13

1 Introduction

Because of null results of experiments aiming to detect dark matter (DM) as a weakly interacting massive particle (WIMP), there is a renewed interest in freeze-in dark matter (FIDM) which differs from WIMP. Compared to WIMP-like DM, a FIDM is produced from the Standard Model (SM) thermal bath of the early Universe via so-called freeze-in mechanism [1], as a result of FIDM feebly coupling to the SM sector.¹ Despite being capable of addressing the observed DM relic density, such feeble coupling makes the FIDM be unlikely to leave observable footprints in the aforementioned experiments, which asks for new detection strategies.

In this work we consider cosmological probes of FIDM. The early studies on effects of DM scattering [2] either off photons or baryons provided Cosmic Microwave Background (CMB) constraints [3–5] being competitive with collider or direct detection limits for WIMP-like DM, which are however not viable for the FIDM. Instead of scattering, DM annihilation or decay into photons and/or electron-positron offers improved CMB constraints [6–16], as a result of

¹To be concrete, we do not consider DM to freeze-in via inflaton sector after the end of inflation.

relevant observables having a lower power laws of the feeble coupling. In this approach, the DM annihilation- or decay-induced energy injection into the intergalactic medium (IGM) modifies ionization history of baryon gas, leading to changes in CMB spectra.

Apart from the imprints in the CMB spectra, DM induced energy injection to the IGM also affects observations of Lyman- α [9, 14, 17, 18] and 21-cm signal [19–22]. Either photons or electron-positron arising from DM annihilation or decay deposit their energies in the IGM via heating, hydrogen ionization, helium single or double ionization and neutral atom excitation, which changes the ionization history of IGM measured by Lyman- α and 21-cm experiments. Compared to the CMB constraints, ref.[18] shows that the Lyman- α lower (upper) bound on DM lifetime (annihilation cross section) can be improved by one-to-two (several) orders of magnitude in certain DM mass range for DM decay (annihilation) into $e\bar{e}$. Similar improved ability of exclusion is also seen in the 21-cm constraints [22]. It is worth noting that these Lyman- α and 21-cm constraints rely on how to model astrophysical reionization and star formation respectively.

Inspired by the reported improvements in simplified DM models, we utilize the observations of Lyman- α and 21-cm signal to place stringent constraints on explicit FIDM model. To derive Lyman- α constraints, we use currently available data about the ionization parameters in low redshift region to infer the astrophysical reionization. Then we use publicly available numerical code to derive FIDM decay or annihilation induced deviations from the baseline values of these ionization parameters in high redshift region. Comparing these deviations to high redshift data gives us the Lyman- α constraints. To derive 21-cm constraints, we follow a standard modeling of star formation developed so far, which gives rise to the baseline values of 21-cm brightness temperature and power spectrum. Likewise, we use publicly available numerical code to calculate FIDM induced deviations from the baseline values of 21-cm power spectrum. Comparing these deviations to future sensitivities on the 21-cm power spectrum in high redshift region, one obtains 21-cm constraints.

The rest of the paper is organized as follows. In Sec.2 we consider the explicit Higgs [23, 24]- and neutrino [25–28]-portal FIDM model, where we derive the FIDM induced energy injection into the IGM, either through its annihilation or decay into $e\bar{e}$ or photon(s). Sec.3 is devoted to model the FIDM induced effects on the evolution of IGM parameters and 21-cm observables, where we briefly introduce theoretical backgrounds and numerical tools adopted for later numerical analysis. In Sec.4 we use the results of Sec.2 to derive the Lyman- α and 21-cm constraints. For the Higgs-portal FIDM model, current Lyman- α data is unable to place efficient constraint while future Lyman- α data on the intergalactic medium temperature with a precision of order $\sim 10\%$ at the redshift range of $z \sim 9 - 15$ is sufficient to exclude this FIDM model. For the neutrino-portal FIDM model, current Lyman- α data has already constrained the DM mass to be less than 1.06 MeV. This surviving DM mass window can be excluded either by future Lyman- α data about the intergalactic medium temperature with a precision of order $\sim 100\%$ at the redshift range of $z \sim 9 - 15$ or future SKA sensitivity (1000 hrs) on the 21-cm power spectrum with respect to reference wavenumber $k_* = 0.2h \text{ Mpc}^{-1}$ at the redshift range of $z \sim 15 - 16$. Finally, we conclude in Sec.5.

2 Freeze-in dark matter induced energy injection into the IGM

In this section we derive the DM induced energy injections into the IGM in two different single-field FIDM models.

2.1 Higgs portal

The first single-field FIDM is built upon the SM Higgs portal with the DM Lagrangian as [23, 24]

$$\mathcal{L}_{\text{dark}} = \frac{1}{2} \partial_\mu X \partial^\mu X - \frac{\mu^2}{2} X^2 - \kappa X^2 |H|^2 - \lambda X^4, \quad (1)$$

where X is the scalar DM, H is the SM Higgs doublet, κ is a small Yukawa coupling between the Higgs and DM, and λ is the self-interacting DM coupling constant. In eq.(1) a hidden Z_2 parity, under which the DM is odd, has been assumed to make sure the completeness of $\mathcal{L}_{\text{dark}}$. We simply ignore the DM self-interaction, as it has no role to play in the following analysis. In the broken electroweak phase the DM mass is given by $m_X^2 = \mu^2 + \kappa v^2$, with $v = 246$ GeV the weak scale. Therefore, the free parameters in this model are only composed of $\{m_X, \kappa\}$.

The left panel of fig.1 presents the observed DM relic abundance $\Omega_X h^2 = 0.12 \pm 0.001$ [29] projected to the plane of $m_X - \kappa$ by using the publicly available code `micrOMEGAs6.0` [30]. In this plot a bump appears near $m_X = m_{h/2}$, pointing to a change in the DM production process. Because in the DM mass range of $m_X < m_{h/2}$ the DM production is dominated by the decay $h \rightarrow \bar{X}X$ with h the physical Higgs scalar, but in the DM mass range of $m_X > m_{h/2}$, where the Higgs decay process is prohibited, the DM production mainly arises from the two-body annihilation of SM particles into $\bar{X}X$ via the virtual Higgs scalar. The required value of DM relic abundance helps us fix the value of κ , with m_X being the only free variable.

The right panel of fig.1 shows the thermally averaged values of cross section of DM annihilation into $e\bar{e}$ as function of m_X , where the value of κ is fixed as in the left panel of fig.1. As the value of m_X increases from $2m_e$ to $m_{h/2}$, the magnitudes of $\langle \sigma v (X\bar{X} \rightarrow e\bar{e}) \rangle$ in units of cm^3/s range from $\sim 10^{-52}$ to $\sim 10^{-56}$, with a resonance taking place near $m_X = m_{h/2}$. Apart from the DM annihilation into $e\bar{e}$, other DM annihilations such as $X\bar{X} \rightarrow p\bar{p}$ may indirectly contribute to the DM induced energy injection into the IGM. Because $p\bar{p}$ subsequently annihilates to stable mesons, $e\bar{e}$ and neutrinos. Taking these effects into account, one can obtain a relatively larger effective value of $\langle \sigma v (\bar{X}X \rightarrow e\bar{e}) \rangle$ for an explicit m_X than in the right panel of fig.1. In this sense $\langle \sigma v (\bar{X}X \rightarrow e\bar{e}) \rangle$ in the right panel provides a conservative estimate on the DM induced energy injection rate via the DM annihilation into $e\bar{e}$.

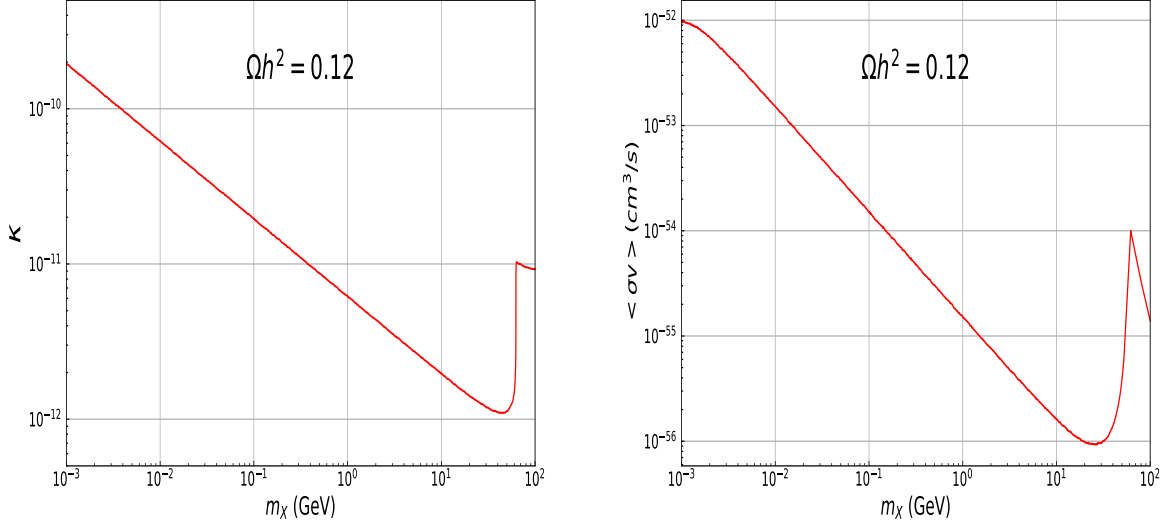


Figure 1: **Left:** the observed DM relic abundance $\Omega_X h^2 = 0.12 \pm 0.001$ projected to the plane of $m_X - \kappa$. **Right:** the thermally averaged values of $\langle \sigma v(X X \rightarrow e \bar{e}) \rangle$, with the value of κ fixed as in the left panel.

2.2 Neutrino portal

The second FIDM model [25–28] is constructed through sterile neutrino with the following DM Lagrangian

$$\mathcal{L} = \bar{N}_I (i\gamma^\mu \partial_\mu - m_I) N_I - Y_{\alpha I} \bar{L}_\alpha \tilde{H} N_I \quad (2)$$

where N_I with $I = 1\text{-}3$ are the right-hand neutrinos ordered in mass, $L_\alpha = (\nu_\alpha, \ell_\alpha)^T$ with $\alpha = 1\text{-}3$ the SM lepton doublets, and $\tilde{H} = i\sigma_2 H^*$ with H the Higgs doublet. In the situation where the lightest active neutrino mass is negligible, the Yukawa coupling $Y_{\alpha 1}$ becomes small, allowing the DM candidate N_1 to freeze-in.

With the heavier sterile neutrinos N_2 and N_3 safely neglected, the freeze-in production of N_1 is dominated by $W^\pm \rightarrow N_1 \ell_\alpha^\pm$. The left plot of fig.2 shows the observed DM relic density projected to the plane of $m_1 - \theta_1$ with $\theta_1^2 = \sum_{\alpha=e,\mu,\tau} (Y_{\alpha 1}^2 v^2 / 2m_1^2)$, which is consistent with the result of [28]. Using this plot to fix the value of θ_1 , we present the decay width of N_1 as function of the DM mass in the right plot of fig.2, using [31–33]

$$\Gamma_{N_1} \approx \Gamma(N_1 \rightarrow \gamma \nu) \approx \frac{9\alpha G_F^2}{1024\pi^4} \sin^2(2\theta_1) m_1^5. \quad (3)$$

The right panel shows the magnitudes of Γ_{N_1} in units of sec^{-1} range from $\sim 10^{-36}$ to $\sim 10^{-20}$ within the DM mass range of $m_1 \sim (10^{-3} - 10)$ MeV. Note that this decay process transfers only a half of the DM rest mass energy into the IGM.

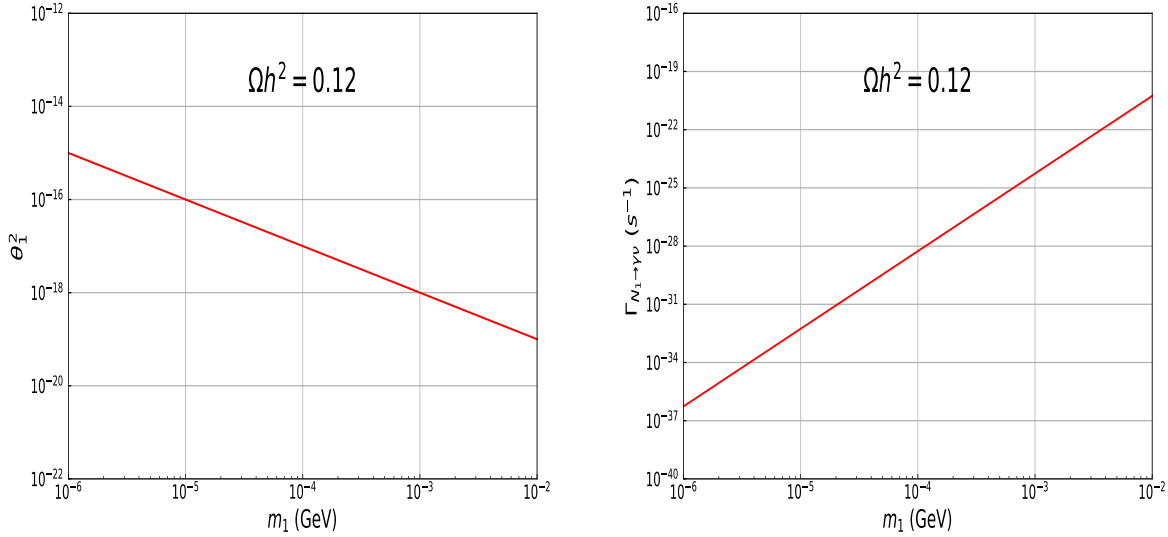


Figure 2: **Left:** the observed DM relic abundance $\Omega_{N_1}h^2 = 0.12 \pm 0.001$ projected to the plane of $m_1 - \theta_1$. **Right:** the decay width of Γ_{N_1} as function of the DM mass m_1 , where the value of θ_1 has been fixed as in the left panel.

3 Modeling dark matter induced effects on cosmological observations

In this section we briefly discuss how to numerically calculate the values of Lyman- α and 21-cm observables from a viewpoint of phenomenology in Sec.3.1 and Sec.3.2 respectively, where we will emphasize the effects of DM annihilation or decay induced energy injection into the IGM on these observables.

3.1 Lyman- α

In the late-time Universe the evolution of IGM ionization fraction and temperature is described by [34]

$$\frac{dx_{\text{HII}}}{dz} = \frac{dt}{dz} (\Lambda_{\text{ion}} - \Lambda_{\text{rec}} + \Lambda_{\text{ion}}^{\text{DM}}), \quad (4)$$

$$\frac{dT_k}{dz} = \frac{2}{3} \frac{T_k}{n_b} \frac{dn_b}{dz} - \frac{T_k}{1+x_e} \frac{dx_e}{dz} + \frac{2}{3k_B(1+x_e)} \frac{dt}{dz} \left(\sum_p \epsilon_{\text{heat}}^p + \epsilon_{\text{heat}}^{\text{DM}} \right), \quad (5)$$

where $x_{\text{HII}} = n_{H^+}/n_H$ is the ionization fraction with n_H (n_{H^+}) the number density of (ionized) hydrogen, T_k the matter (baryon) temperature, n_b the baryon number density, k_B the Boltzmann constant, and z the redshift. In eq.(4), Λ_{ion} includes the photoionization and

astrophysical source induced ionization rate, Λ_{rec} is the recombination rate, and $\Lambda_{\text{ion}}^{\text{DM}}$ represents the DM-induced ionization rate. In eq.(5), ϵ_{heat}^p includes the Compton scattering (effective at $z \geq 300$) and astrophysical source induced heating rate, and $\epsilon_{\text{heat}}^{\text{DM}}$ is the DM induced heating rate.

The DM annihilation or decay induced terms in eqs.(4) and (5) are given by [22, 34]

$$\epsilon_c^{\text{DM}} = f_c(x_e, z) \frac{1}{n_b} \left(\frac{dE(z)}{dt dV} \right)_{\text{inj}}, \quad (6)$$

$$\Lambda_{\text{ion}}^{\text{DM}} = \mathcal{F}_{\text{H}} \frac{\epsilon_{\text{HII}}^{\text{DM}}}{E_{\text{th}}^{\text{HII}}} + \mathcal{F}_{\text{He}} \frac{\epsilon_{\text{HeII}}^{\text{DM}}}{E_{\text{th}}^{\text{HeII}}}, \quad (7)$$

where $f_c(x_e, z)$ are the deposition fractions, with deposition channels including IGM heating ($c=\text{heat}$), hydrogen ionization ($c = \text{HII}$), helium single or double ionization ($c = \text{HeII}$ or HeIII), and neutral atom excitation ($c = \text{exc}$), \mathcal{F}_j refers to the number fraction of each species j , E_{th}^j is the energy for ionization. In eq.(6) the DM induced energy injection rate is defined as

$$\left(\frac{dE(z)}{dt dV} \right)_{\text{inj}} = \begin{cases} \rho_{\text{DM},0}^2 (1+z)^6 \langle \sigma v \rangle / m_{\text{DM}}, & \text{annihilation} \\ \rho_{\text{DM},0} (1+z)^3 \Gamma_{\text{DM}}, & \text{decay} \end{cases} \quad (8)$$

where $\langle \sigma v \rangle$ is the velocity-averaged DM annihilation cross section, Γ_{DM} the DM decay width, $\rho_{\text{DM},0}$ the present value of DM relic density, and m_{DM} the DM mass.

Given an explicit DM model, the energy injection rates in eq.(8) are specified as illustrated in Sec.2. Taking these rates as inputs, we use the publicly available package `DarkHistory` [34, 35] to calculate the deposition fractions $f_c(x_e, z)$ in eq.(6) and to derive the Lyman- α limits on the DM annihilation or decay rate. In particular, `DarkHistory`

- uses $x_e = n_e/n_H$, with n_e the number density of free electron;
- chooses the case-B photoionization and recombination coefficients for hydrogen;
- allows us to parametrize the astrophysical source contributing to photoionization and photoheating.

3.2 21-cm signal

Now we turn to 21-cm cosmology.² Instead of eq.(4) it is more common to use

$$\frac{dx_e}{dz} = \frac{dt}{dz} (\Lambda_{\text{ion}} - \Lambda_{\text{rec}} + \Lambda_{\text{ion}}^{\text{DM}}). \quad (9)$$

²For a review see [36].

Just like T_k in eq.(5), the Wouthuysen-Field coupling x_α is also modified by any exotic energy injection involved,

$$x_\alpha = 1.7 \times 10^{11} \frac{S_\alpha}{1 + z \text{ s}^{-1} \text{Hz}^{-1} \text{cm}^{-2} \text{sr}^{-1}} \frac{J_\alpha}{\text{cm}^{-2} \text{sr}^{-1}} \quad (10)$$

where S_α is a correction coefficient [37] of order unity, and J_α is the Lyman- α background density

$$J_\alpha \rightarrow J_\alpha + J_\alpha^{\text{DM}}, \quad (11)$$

with DM induced Lyman- α intensity [22]

$$J_\alpha^{\text{DM}} = \frac{cn_b}{4\pi H(z)\nu_\alpha} \frac{\epsilon_{\text{Ly}\alpha}}{h\nu_\alpha}. \quad (12)$$

Here, H is the Hubble rate, ν_α the Lyman- α frequency and $\epsilon_{\text{Ly}\alpha}$ the DM induced Lyman- α excitation.

Using eqs.(5), (9) and (10), one is able to derive the effects of DM induced energy injection into the IGM on the spin temperature

$$T_S^{-1} = \frac{T_{\text{CMB}}^{-1} + (x_\alpha + x_c)T_k^{-1}}{1 + x_\alpha + x_c}, \quad (13)$$

where x_c is the collision coupling. Given the value of T_S in eq.(13), it is straightforward to determine the differential brightness temperature of 21-cm signal arising from the hyperfine spin-flip transition of neutral hydrogen [38]

$$\delta T_{21}(z) \approx 20x_{\text{HI}}(1 + \delta_b) \left(1 - \frac{T_{\text{CMB}}}{T_S}\right) \left(\frac{1+z}{10}\right)^{1/2} \left(\frac{\Omega_b h^2}{0.023}\right) \left(\frac{\Omega_m h^2}{0.15}\right)^{-1/2} \text{ mK}, \quad (14)$$

where x_{HI} is the neutral hydrogen fraction, δ_b is the baryon over density, Ω_b and Ω_m are the baryon and matter energy density relative to the present critical density respectively, and the Hubble parameter h is defined as $H_0 = h \cdot 100 \text{ km s}^{-1} \text{Mpc}^{-1}$ with H_0 the present-day Hubble rate.

Apart from the global 21-cm signal, spatial variation of IGM quantities leads to fluctuations in the 21-cm signal. The 21-cm power spectrum is defined as

$$\overline{\delta T_{21}^2} \Delta_{21}^2(k, z) = \overline{\delta T_{21}^2(z)} \times \frac{k^3}{2\pi^2} P_{21}(k, z) \quad (15)$$

where $\overline{\delta T_{21}}$ is the sky-averaged brightness temperature and P_{21} is given by

$$\left\langle \tilde{\delta}_{21}(\mathbf{k}, z) \tilde{\delta}_{21}(\mathbf{k}', z) \right\rangle = (2\pi)^3 \delta^D(\mathbf{k}' - \mathbf{k}) P_{21}(k, z) \quad (16)$$

with $\tilde{\delta}_{21}(\mathbf{k}, z)$ the Fourier transformation of $\delta_{21}(\mathbf{x}, z) = \delta T_{21}(\mathbf{x}, z) / \overline{\delta T_{21}}(z) - 1$.

To derive 21-cm limit on DM induced energy injection, we use the package **DM21cm** [39]³ which combines **DarkHistory** and **21cmFAST** [40, 41]. Explicitly, **DM21cm**

³The current version of this package is only viable to deal with DM decay induced energy injection into the IGM.

- follows the convention $x_e = n_e/n_b$;
- chooses the case-A photoionization and recombination coefficients for hydrogen;
- parametrizes the astrophysical source in terms of modeling star formation.

DM21cm uses `DarkHistory` to calculate transfer functions which depend on δ_b , x_{HI} , T_k , incident photon flux etc for each location in the simulation volume at redshift z_i . Over the interval z_i to z_{i+1} , the transfer functions are then used to generate a new uniform photon bath and X-ray luminosity field, and the energy deposition fields obtained from `DarkHistory` are combined with `21cmFAST` to yield a new simulation state of `21cmFAST` containing the information of x_e , T_k and δ_b . Repeating this process, we obtain the evolution of those IGM parameters as function of z . With respect to each z , the 21-cm power spectrum $\Delta_{21}^2(k, z)$ is derived in terms of `21cmFAST`.

4 Results

In this section we present the Lyman- α and 21-cm limits on the two single-field FIDM models discussed in Sec.2.

4.1 Higgs portal

4.1.1 Lyman- α

The **top** panel of fig.3 shows the baseline ionization history (in black) of ionization fraction x_e (left) and IGM temperature T_k (right) as function of redshift z . The baseline ionization history is inferred from the astrophysical reionization constrained by the Planck data [29] about x_e and the data [42, 43] about T_k as follows. Similar to [18] we adopt the FlexKnot model to parametrize the astrophysical source contribution to Λ_{ion} in eq.(4) and a photoheated prescription to parametrize the astrophysical source contribution to ϵ_{heat}^p in eq.(5) simultaneously. Using the data [42, 43] on T_k in the low redshift range of $z \sim 4 - 7$, the parameters $(\Delta T, \alpha_{\text{bk}})$ in the photoheated prescription can be fixed [18]. So, a combination of the Planck data [29] and the data [42, 43] enables us to determine the astrophysical reionization. Using `DarkHistory`, it is straightforward to extend this baseline astrophysical reionization to higher redshift regions, which gives us the so-called baseline ionization history. Alongside the baseline ionization history, we also show the evolution of x_e and T_k with the Higgs-portal FIDM annihilation induced energy injection into the IGM taken into account for various values of DM mass $m_X = \{10^{-3}, 10^{-2}, 10^2\}$ GeV using the right plot of fig.1.

The **bottom** panel of fig.3 presents the FIDM annihilation induced derivations from the baseline values of x_e (left) and T_k (right) for the benchmark DM masses in the top panel of fig.3. Two comments are in order regarding the plots therein. (i) The significant changes

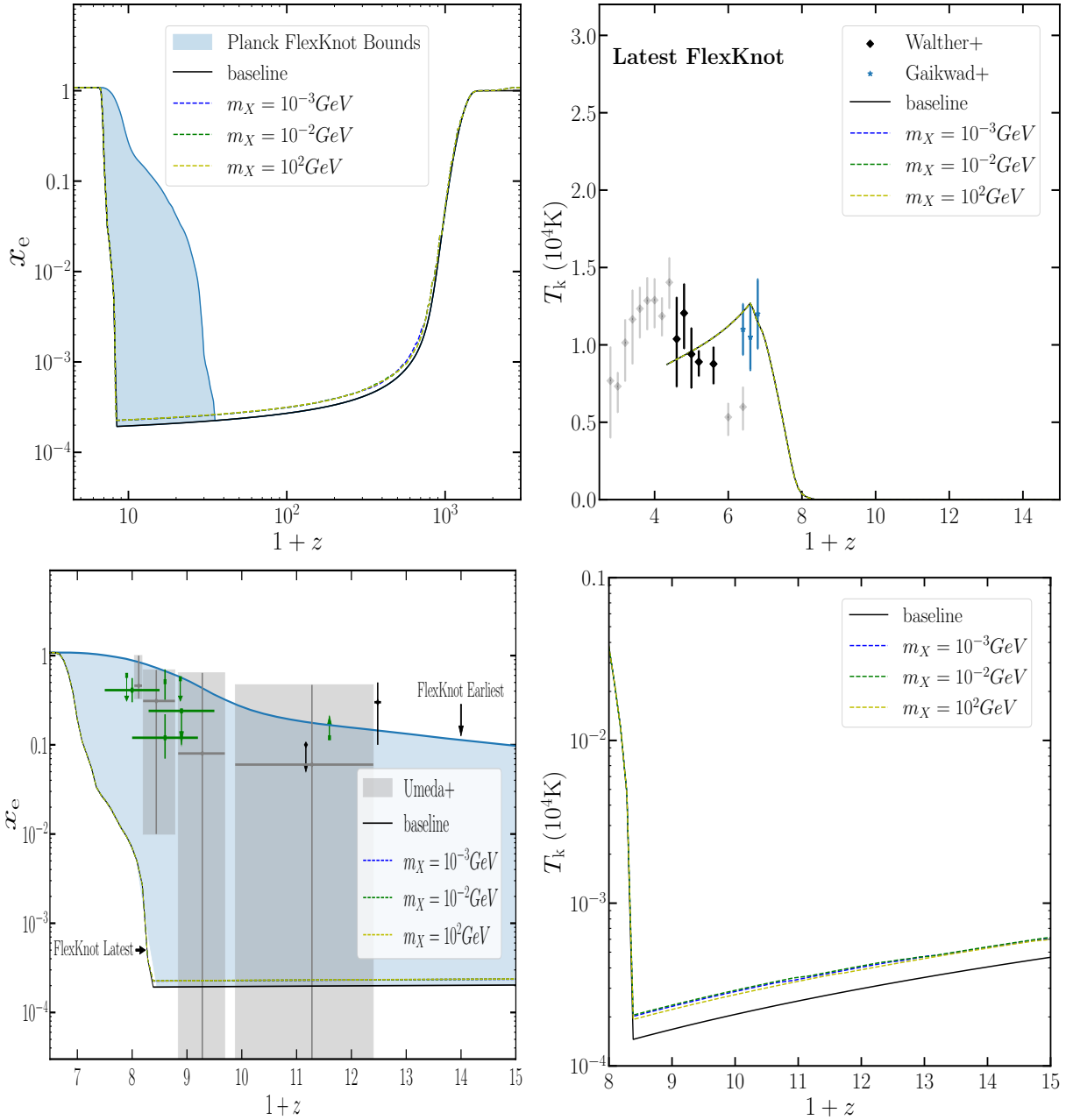


Figure 3: **Top:** the baseline ionization history (in black) of x_e (left) and T_k (right) based upon the FlexKnot model and photoheated parametrization with parameter values $(\Delta T, \alpha_{\text{bk}}) = (24665\text{K}, 0.57)$ [18] fixed by the data from Walther+ [42] (black diamonds) and Gaikwad+ [43] (blue stars) in the redshift range of $z \sim 4 - 7$. Alongside the baseline ionization history, we also present the Higgs-portal FIDM annihilation induced effects on the evolution of these two parameters for various values of DM mass $m_X = \{10^{-3}, 10^{-2}, 10^2\}$ GeV using fig.1. **Bottom:** we zoom in the deviations from the baseline values of x_e (left) and T_k (right) in high redshift region for the benchmark DM masses in the top panel, as compared to the JWST constraint on x_e from Umeda+ [44] (in shaded gray) among others. A combination of the Planck, Walther+, Gaikwad+ and Umeda+ data cannot exclude this Higgs-portal FIDM model. See the text for details.

in the evolution of x_e and T_k occur at certain values z_* which refers to the beginning of the astrophysical reionization. (ii) Compared to the JWST constraint on x_e in the high redshift range of $z \sim 7.0 - 11.4$ from Umeda+ data [44] (shaded gray) via Lyman- α damping wing absorptions in 26 bright continuum galaxies, this Higgs-portal FIDM, which lives in nearly the entire FlexKnot region with the left and right boundary known as the latest and earliest FlexKnot reionization, cannot be excluded. Here, we also show the other JWST constraints from Lyman- α damping wing absorption profile of individual UV spectrum of galaxies [45, 46] (in black diamonds) and from Lyman- α of Lyman-break galaxies [47, 48] (in green squares), which are basically covered by the shaded gray region.

A future data about T_k in the high redshift range can improve the ability of exclusion. For example, a precision of order $\sim 10\%$ in the baseline values of T_k within the redshift range of $z \sim 8.5 - 15$ is sufficient to discriminate the DM induced effect on T_k from the baseline values of T_k .

4.2 Neutrino portal

4.2.1 Lyman- α

Restricting to the astrophysical reionization the **top** panel of fig.4 shows the baseline ionization history (in black) of x_e (left) and T_k (right) as function of redshift z . Apart from the baseline ionization history, we also show the evolution of x_e and T_k with the neutrino-portal FIDM decay induced energy injection into the IGM taken into account for various values of DM mass $m_1 = \{0.546, 1.06, 1.95, 2.40, 2.63\}$ MeV using the right plot of fig.2. There the plot of T_k has already constrained the DM mass to $m_1 \leq 1.06$ MeV by requiring that the DM decay induced contribution to T_k is smaller than its baseline value within the redshift range of $z \sim 4 - 7$.

In the **bottom** panel of fig.4 we zoom in the FIDM induced deviations in x_e (left) and T_k (right) from their baseline values for the benchmark DM masses as shown in the top panel. There the values of x_e have been compared to the Umeda+ data on x_e from Lyman- α damping wing absorptions in 26 bright continuum galaxies [44] (in shaded gray region) in the high redshift range of $z \sim 7.0 - 11.4$. While being consistent with the Umeda+ data, the bottom panel shows that DM mass $m_1 \geq 1.06$ MeV can be excluded by $x_e \leq 10^{-2}$ in the redshift range of $z \sim 9 - 12$. On the contrary, if $x_e \geq 10^{-2}$ within this redshift region, which is probably confirmed by future JWST data, the surviving DM mass window cannot be excluded at all.

Even so future data about T_k can shed light on the surviving DM mass window with $m_1 \leq 1.06$ MeV. The plot of T_k in the bottom panel of fig.4 shows that the values of T_k within the surviving DM mass window are about one-to-two orders of magnitude larger than the baseline values of T_k in the redshift region of $z \sim 9 - 15$. This suggests that the measurements on T_k with a precision of order 100% within this redshift region are able to exclude the surviving DM mass window.

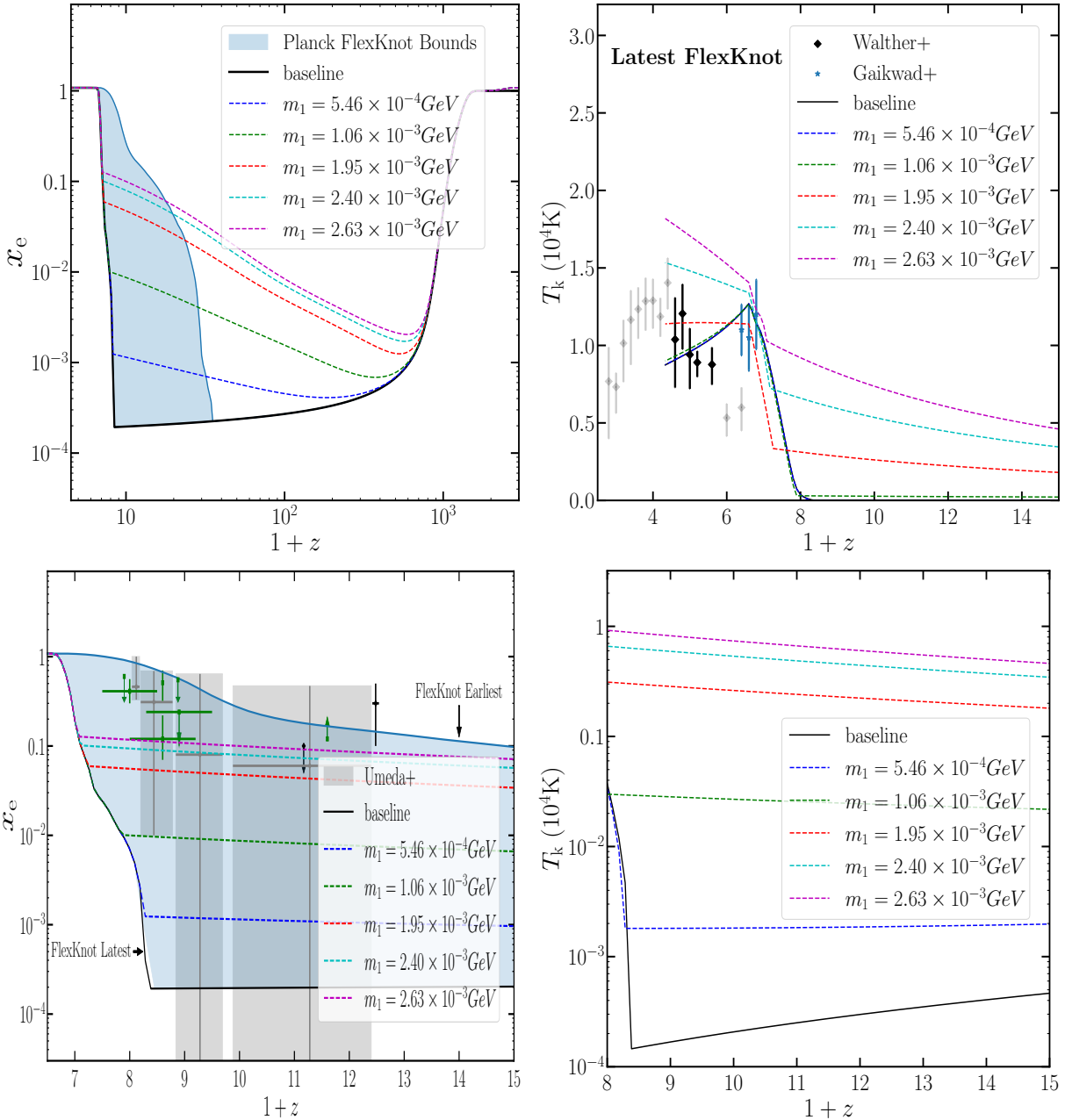


Figure 4: **Top:** the baseline ionization history (in black) of x_e (left) and T_k (right) based upon the FlexKnot model and photoheated parametrization as in fig.3. Besides the baseline ionization history, we also present the neutrino-portal FIDM decay induced effects on the evolution of these two IGM parameters for various values of DM mass $m_1 = \{0.546, 1.06, 1.95, 2.40, 2.63\}$ MeV using fig.2. **Bottom:** we zoom in the deviations from the baseline values of x_e (left) and T_k (right) in high redshift region for the benchmark DM masses in the top panel, as compared to the Umeda+ [44] (in shaded gray) among others. A combination of the Planck, Walther+, Gaikwad+ and Umeda+ excludes this neutrino-portal FIDM model except a DM mass window with $m_1 \leq 1.06$ MeV. See the text for details.

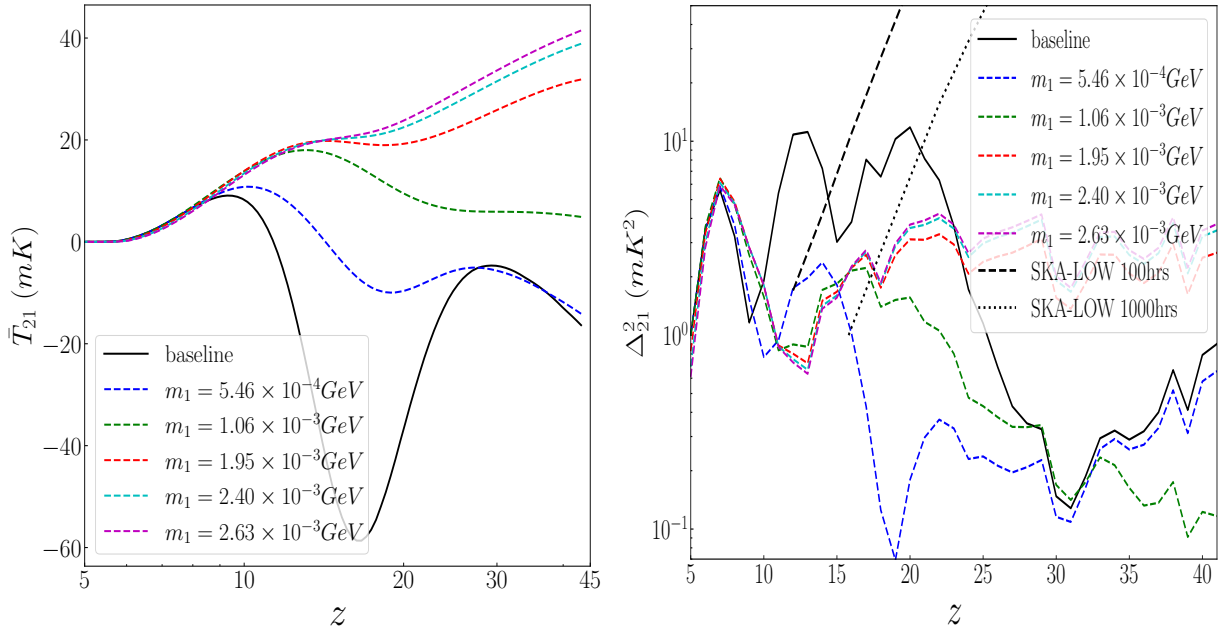


Figure 5: **Left:** the baseline values of $\langle T_{21} \rangle$ (in black) as function of z and the deviations from them due to the neutrino-portal FIDM decay induced effects on the IGM for various values of DM mass m_1 . **Right:** the same as the left panel but for the 21-cm power spectrum Δ_{21}^2 with respect to the reference wavenumber $k_* = 0.2h \text{ Mpc}^{-1}$, compared to future SKA [58] sensitivities with respect to 100 hrs (in black dashed) and 1000 hrs (in black dotted) simultaneously, which implies that a precision of order $\sim 10\%$ in $\Delta_{21}^2(k_*)$ in the redshift range of $z \sim 15 - 16$ provided by SKA (1000 hrs) is sufficient to exclude the surviving DM mass window uncovered by the Lyman- α constraint in fig.4.

4.2.2 21-cm signal

The **left** panel of fig.5 shows the global values of $\langle T_{21} \rangle$ as function of z . In this plot the baseline values of $\langle T_{21} \rangle$ (in black) arises from the standard astrophysical processes such as stellar emission of UV and X-ray photons leading to energy deposition into heating, ionization and Lyman- α excitation, which are modeled by 21cmFAST with fiducial values of 21cmFAST parameters taken from [49, 50]. Meanwhile, this plot also shows the FIDM decay induced deviations from the baseline values of $\langle T_{21} \rangle$ with respect to various values of DM mass using fig.2. While EDGES [51] reported a measurement on $\langle T_{21} \rangle$, it however disputes with SARAS3 [52] among others. Therefore, we do not make use of this data for the present analysis but instead consider the sensitivities of future experiments on the 21-cm power spectrum as below.

The **right** panel of fig.5 shows the values of the 21-cm power spectrum Δ_{21}^2 as function of z with respect to the reference wavenumber $k_* = 0.2h \text{ Mpc}^{-1}$. Explicitly, we have chosen a comoving volume of $(256 \text{ Mpc})^3$ with a comoving grid resolution of 2 Mpc and a redshift

interval of $\delta z = 1$ for the T_{21} lightcones. This panel shows that the FIDM decay induced deviations from the baseline values of $\Delta_{21}^2(k_*)$ are small in low redshift region ($z \leq 10$) but large in the high redshift range of $z > 10$. This feature is consistent with the previous results of [39]. Consider that these deviations are far below current LOFAR [53, 54] and HERA [55, 56] limits, we compare them to future HERA [57] and SKA [58, 59] experiment. While beyond the expected sensitivity of HERA which is not shown here, the surviving DM mass window uncovered by the Lyman- α constraint in fig.4 can be excluded by a precision of order $\sim 10\%$ in $\Delta_{21}^2(k_*)$ in the redshift range of $z \sim 15 - 16$ provided by SKA (1000 hrs).

5 Conclusion

In this work we have derived both the Lyman- α and 21-cm constraints on two single-field FIDM models that are beyond the reaches of conventional DM detection experiments. Regarding the Lyman- α constraint, with the astrophysical reionization fixed by the Planck, Walther+ and Gaikwad+ data, the Umeda+ data on x_e is unable to place efficient constraint on the Higgs-portal FIDM as a result of the small deviations from the baseline ionization history, which can however be excluded by future Lyman- α data on T_k with a $\sim 10\%$ precision at the redshift range of $z \sim 9 - 15$, whereas a combination of the Planck, Walther+, Gaikwad+ and Umeda+ data has already constrained the neutrino-portal FIDM mass to be less than 1.06 MeV, which can be excluded by future Lyman- α data about T_k with an $\sim 100\%$ precision at the redshift range of $z \sim 9 - 15$. For the 21-cm constraint, we have shown that the surviving neutrino-portal FIDM mass window can be also excluded by the future SKA sensitivity (1000 hrs) on the 21-cm power spectrum with respect to $k_* = 0.2h \text{ Mpc}^{-1}$ at the redshift range of $z \sim 15 - 16$.

Several factors affect the derived exclusions. For the Lyman- α constraints, the baseline ionization history with respect to the astrophysical reionization relies on the Walther+ and Gaikwad+ data. Using a set of data points different from [18] which we follow here may mildly change the baseline ionization history. Alternatively, one can even replace the astrophysical reionization by DM reionization. In this situation, the Walther+ and Gaikwad+ data allow a larger DM contribution to T_k at $z \sim 4 - 6$, which implies a larger x_e at high redshift region accordingly. For the 21-cm constraints, DM21cm has followed 21cmFAST to adopt two stellar populations, each of which contains several parameters. If one takes fiducial values of the 21cmFAST parameters different from [49, 50], the baseline values of 21-cm power spectrum are expected to be modified. Finally, as emphasized in the Higgs-portal FIDM model, the annihilation or decay of FIDM into SM final states rather than $e\bar{e}$ and photons may indirectly contribute to the FIDM induced deviations from the baseline values of Lyman- α and 21-cm observables.

Our approach can be applied to other FIDM models. Take axion-like DM extensively studied in the literature for example. It mainly decays into photons similar to the neutrino-portal FIDM considered here. Both the Lyman- α and 21-cm constraints on the axion-like DM can be similarly derived given its freeze-in processes identified [60]. Likewise, this approach

can be also applied to two-field FIDM models such as [61] where DM annihilates or decays into $e\bar{e}$ or photons. These constraints may be more competitive than other considerations in certain DM mass region.

References

- [1] L. J. Hall, K. Jedamzik, J. March-Russell and S. M. West, JHEP **03** (2010), 080, [arXiv:0911.1120 [hep-ph]].
- [2] F. Y. Cyr-Racine, K. Sigurdson, J. Zavala, T. Bringmann, M. Vogelsberger and C. Pfrommer, Phys. Rev. D **93**, no.12, 123527 (2016), [arXiv:1512.05344 [astro-ph.CO]].
- [3] C. Dvorkin, K. Blum and M. Kamionkowski, Phys. Rev. D **89**, no.2, 023519 (2014), [arXiv:1311.2937 [astro-ph.CO]].
- [4] W. L. Xu, C. Dvorkin and A. Chael, Phys. Rev. D **97**, no.10, 103530 (2018), [arXiv:1802.06788 [astro-ph.CO]].
- [5] T. R. Slatyer and C. L. Wu, Phys. Rev. D **98**, no.2, 023013 (2018), [arXiv:1803.09734 [astro-ph.CO]].
- [6] N. Padmanabhan and D. P. Finkbeiner, Phys. Rev. D **72**, 023508 (2005), [arXiv:astro-ph/0503486 [astro-ph]].
- [7] T. R. Slatyer, N. Padmanabhan and D. P. Finkbeiner, Phys. Rev. D **80**, 043526 (2009), [arXiv:0906.1197 [astro-ph.CO]].
- [8] L. Lopez-Honorez, O. Mena, S. Palomares-Ruiz and A. C. Vincent, JCAP **07**, 046 (2013), [arXiv:1303.5094 [astro-ph.CO]].
- [9] R. Diamanti, L. Lopez-Honorez, O. Mena, S. Palomares-Ruiz and A. C. Vincent, JCAP **02**, 017 (2014), [arXiv:1308.2578 [astro-ph.CO]].
- [10] T. R. Slatyer, Phys. Rev. D **93**, no.2, 023521 (2016), [arXiv:1506.03812 [astro-ph.CO]].
- [11] V. Poulin, P. D. Serpico and J. Lesgourgues, JCAP **12**, 041 (2015), [arXiv:1508.01370 [astro-ph.CO]].
- [12] C. Dvorkin, T. Lin and K. Schutz, Phys. Rev. Lett. **127**, no.11, 111301 (2021), [arXiv:2011.08186 [astro-ph.CO]].
- [13] B. Bolliet, J. Chluba and R. Battye, Mon. Not. Roy. Astron. Soc. **507**, no.3, 3148-3178 (2021), [arXiv:2012.07292 [astro-ph.CO]].
- [14] F. Capozzi, R. Z. Ferreira, L. Lopez-Honorez and O. Mena, JCAP **06**, 060 (2023), [arXiv:2303.07426 [astro-ph.CO]].

[15] H. Liu, W. Qin, G. W. Ridgway and T. R. Slatyer, Phys. Rev. D **108**, no.4, 043531 (2023), [arXiv:2303.07370 [astro-ph.CO]].

[16] S. P. Li, [arXiv:2402.16708 [hep-ph]].

[17] H. Liu, T. R. Slatyer and J. Zavala, Phys. Rev. D **94** (2016) no.6, 063507, [arXiv:1604.02457 [astro-ph.CO]].

[18] H. Liu, W. Qin, G. W. Ridgway and T. R. Slatyer, Phys. Rev. D **104**, no.4, 043514 (2021), [arXiv:2008.01084 [astro-ph.CO]].

[19] H. Liu and T. R. Slatyer, Phys. Rev. D **98** (2018) no.2, 023501, [arXiv:1803.09739 [astro-ph.CO]].

[20] G. D'Amico, P. Panci and A. Strumia, Phys. Rev. Lett. **121** (2018) no.1, 011103, [arXiv:1803.03629 [astro-ph.CO]].

[21] A. Mitridate and A. Podo, JCAP **05** (2018), 069, [arXiv:1803.11169 [hep-ph]].

[22] G. Facchinetti, L. Lopez-Honorez, Y. Qin and A. Mesinger, [arXiv:2308.16656 [astro-ph.CO]].

[23] J. McDonald, Phys. Rev. Lett. **88**, 091304 (2002), [arXiv:hep-ph/0106249 [hep-ph]].

[24] Z. Kang, Phys. Lett. B **751**, 201-204 (2015), [arXiv:1505.06554 [hep-ph]].

[25] T. Asaka, K. Ishiwata and T. Moroi, Phys. Rev. D **73**, 051301 (2006), [arXiv:hep-ph/0512118 [hep-ph]].

[26] M. Becker, Eur. Phys. J. C **79**, no.7, 611 (2019), [arXiv:1806.08579 [hep-ph]].

[27] M. Chianese and S. F. King, JCAP **09**, 027 (2018), [arXiv:1806.10606 [hep-ph]].

[28] A. Datta, R. Roshan and A. Sil, Phys. Rev. Lett. **127**, no.23, 231801 (2021), [arXiv:2104.02030 [hep-ph]].

[29] N. Aghanim *et al.* [Planck], Astron. Astrophys. **641**, A6 (2020) [erratum: Astron. Astrophys. **652**, C4 (2021)], [arXiv:1807.06209 [astro-ph.CO]].

[30] G. Alguero, G. Belanger, F. Boudjema, S. Chakraborti, A. Goudelis, S. Kraml, A. Mjalal and A. Pukhov, Comput. Phys. Commun. **299**, 109133 (2024), [arXiv:2312.14894 [hep-ph]].

[31] P. B. Pal and L. Wolfenstein, Phys. Rev. D **25**, 766 (1982)

[32] V. D. Barger, R. J. N. Phillips and S. Sarkar, Phys. Lett. B **352**, 365-371 (1995) [erratum: Phys. Lett. B **356**, 617-617 (1995)], [arXiv:hep-ph/9503295 [hep-ph]].

- [33] A. Boyarsky, O. Ruchayskiy and M. Shaposhnikov, Ann. Rev. Nucl. Part. Sci. **59**, 191-214 (2009), [arXiv:0901.0011 [hep-ph]].
- [34] H. Liu, G. W. Ridgway and T. R. Slatyer, Phys. Rev. D **101**, no.2, 023530 (2020), [arXiv:1904.09296 [astro-ph.CO]].
- [35] Y. Sun and T. R. Slatyer, Phys. Rev. D **107**, no.6, 063541 (2023), [arXiv:2207.06425 [hep-ph]].
- [36] J. R. Pritchard and A. Loeb, Rept. Prog. Phys. **75** (2012), 086901, [arXiv:1109.6012 [astro-ph.CO]].
- [37] C. M. Hirata, Mon. Not. Roy. Astron. Soc. **367**, 259-274 (2006), [arXiv:astro-ph/0507102 [astro-ph]].
- [38] S. Furlanetto, S. P. Oh and F. Briggs, Phys. Rept. **433**, 181-301 (2006), [arXiv:astro-ph/0608032 [astro-ph]].
- [39] Y. Sun, J. W. Foster, H. Liu, J. B. Muñoz and T. R. Slatyer, [arXiv:2312.11608 [hep-ph]].
- [40] A. Mesinger, S. Furlanetto and R. Cen, Mon. Not. Roy. Astron. Soc. **411**, 955 (2011), [arXiv:1003.3878 [astro-ph.CO]].
- [41] S. G. Murray, B. Greig, A. Mesinger, J. B. Muñoz, Y. Qin, J. Park and C. A. Watkinson, J. Open Source Softw. **5**, no.54, 2582 (2020), [arXiv:2010.15121 [astro-ph.IM]].
- [42] M. Walther, J. Oñorbe, J. F. Hennawi and Z. Lukić, Astrophys. J. **872** (2019) no.1, 13, [arXiv:1808.04367 [astro-ph.CO]].
- [43] P. Gaikwad, M. Rauch, M. G. Haehnelt, E. Puchwein, J. S. Bolton, L. C. Keating, G. Kulkarni, V. Iršič, E. Bañados and G. D. Becker, *et al.* Mon. Not. Roy. Astron. Soc. **494** (2020) no.4, 5091-5109, [arXiv:2001.10018 [astro-ph.CO]].
- [44] H. Umeda, *et al.* [arXiv:2306.00487[astro-ph.GA]].
- [45] E. Curtis-Lake, *et al.* [arXiv:2212.04568 [astro-ph.GA]].
- [46] T. Y. Y. Hsiao, Abdurro'uf, D. Coe, R. L. Larson, I. Jung, M. Mingozi, P. Dayal, N. Kumari, V. Kokorev and A. Vikaeus, *et al.* [arXiv:2305.03042 [astro-ph.GA]].
- [47] T. Morishita, *et al.* [arXiv:2211.09097 [astro-ph.GA]].
- [48] S. Bruton, *et al.* [arXiv:2303.03419 [astro-ph.GA]].
- [49] J. B. Muñoz, Y. Qin, A. Mesinger, S. G. Murray, B. Greig and C. Mason, Mon. Not. Roy. Astron. Soc. **511**, no.3, 3657-3681 (2022), [arXiv:2110.13919 [astro-ph.CO]].

- [50] C. A. Mason, J. B. Muñoz, B. Greig, A. Mesinger and J. Park, [arXiv:2212.09797 [astro-ph.CO]].
- [51] J. D. Bowman, A. E. E. Rogers, R. A. Monsalve, T. J. Mozdzen and N. Mahesh, *Nature* **555** (2018) no.7694, 67-70, [arXiv:1810.05912 [astro-ph.CO]].
- [52] S. Singh, J. Nambissan T., R. Subrahmanyam, N. Udaya Shankar, B. S. Girish, A. Raghunathan, R. Somashekhar, K. S. Srivani and M. Sathyanaarayana Rao, *Nature Astron.* **6**, no.5, 607-617 (2022).
- [53] A. H. Patil, S. Yatawatta, L. V. E. Koopmans, A. G. de Bruyn, M. A. Brentjens, S. Zaroubi, K. M. B. Asad, M. Hatef, V. Jelić and M. Mevius, *et al.* *Astrophys. J.* **838**, no.1, 65 (2017), [arXiv:1702.08679 [astro-ph.CO]].
- [54] F. G. Mertens, M. Mevius, L. V. E. Koopmans, A. R. Offringa, G. Mellema, S. Zaroubi, M. A. Brentjens, H. Gan, B. K. Gehlot and V. N. Pandey, *et al.* *Mon. Not. Roy. Astron. Soc.* **493**, no.2, 1662-1685 (2020), [arXiv:2002.07196 [astro-ph.CO]].
- [55] Z. Abdurashidova *et al.* [HERA], *Astrophys. J.* **925** (2022) no.2, 221, [arXiv:2108.02263 [astro-ph.CO]].
- [56] Z. Abdurashidova *et al.* [HERA], *Astrophys. J.* **945**, no.2, 124 (2023), [arXiv:2210.04912 [astro-ph.CO]].
- [57] J. B. Muñoz, C. Dvorkin and A. Loeb, *Phys. Rev. Lett.* **121**, no.12, 121301 (2018), [arXiv:1804.01092 [astro-ph.CO]].
- [58] F. G. Mertens, B. Semelin and L. V. E. Koopmans, [arXiv:2109.10055 [astro-ph.CO]].
- [59] L. V. E. Koopmans, J. Pritchard, G. Mellema, F. Abdalla, J. Aguirre, K. Ahn, R. Barkana, I. van Bemmel, G. Bernardi and A. Bonaldi, *et al.* *PoS AASKA14*, 001 (2015), [arXiv:1505.07568 [astro-ph.CO]].
- [60] M. Jain, A. Maggi, W. Y. Ai and D. J. E. Marsh, [arXiv:2406.01678 [hep-ph]].
- [61] X. Yin, S. Xu and S. Zheng, [arXiv:2311.10360 [hep-ph]].